GASTROENTEROLOGY 2011;140:1556–1563

JNK Signaling Promotes Intestinal Tumorigenesis Through Activation of mTOR Complex 1 in *Apc*$^{\Delta 716}$ Mice

TERUAKI FUJISHITA, MASAHIRO AOKI, and MAKOTO M. TAKETO

Department of Pharmacology, Graduate School of Medicine, Kyoto University, Yoshida-Konoé-Cho, Sakyo-Ku, Kyoto, Japan

See editorial on page 1387.

BACKGROUND & AIMS: Signaling by the mammalian target of rapamycin complex 1 (mTORC1) has been implicated in various human cancers. mTORC1 signaling is activated in intestinal tumors of adenomatous polyposis coli (*Apc*$^{\Delta 716}$) mice, a model of familial adenomatous polyposis; in these mice, the mTORC1 inhibitor RAD001 can block tumor formation. However, the precise mechanism of mTORC1 signaling in intestinal tumors is not clear. We investigated whether c-Jun-NH_2 terminal kinase (JNK) is involved in the mTORC1 activation. **METHODS:** We investigated the effects of an inhibitor and an activator of JNK, as well as small interfering RNA against JNK, on mTORC1 in *Apc*$^{\Delta 716}$ mice and colon cancer cell lines. We also determined the role of JNK in mTORC1 signaling using in vitro kinase assays. **RESULTS:** JNK was activated in intestinal polyps of *Apc*$^{\Delta 716}$ mice; the JNK inhibitor SP600125 significantly suppressed tumor formation. In colorectal cancer cell lines, the JNK activator anisomycin activated mTORC1, whereas SP600125 or small interfering RNAs against JNK suppressed signaling. Importantly, JNK stimulated the mTORC1 kinase activity in vitro, through direct phosphorylation of Raptor at serine 863. **CONCLUSIONS: JNK is required for activation of mTORC1 in intestinal tumor cells. JNK inhibitors might be developed as therapeutics or to prevent development of intestinal tumors.**

Keywords: mTORC1; JNK; Intestinal Tumor.

BASIC—ALIMENTARY TRACT

Mammalian target of rapamycin (mTOR) is a serine/threonine kinase that can form 2 complexes with distinct functions: mTORC1 and mTORC2.[1] Although mTORC1 is composed of mTOR, Raptor, and mLST8 (and PRAS40), mTORC2 consists of mTOR, Rictor, mLST8, mSin1, and Protor.[2] It is known that mTORC1 phosphorylates p70 s6 kinase (S6K) and eukaryotic initiation factor 4E-binding protein 1 (4EBP1), and thereby enhances translation of subsets of messenger RNAs (mRNAs). Activation of mTORC1 signaling thus promotes protein synthesis and cell growth. On the other hand, mTORC2 can phosphorylate Akt and serum/glucocorticoid regulated kinase, and promote actin organization as well.[2]

Although prototypic mTORC1 inhibitor sirolimus (rapamycin) has been used as an immunosuppressive agent to prevent rejection of transplanted organs, its derivatives have been tested for cancer therapy because of their growth-inhibitory effects. Namely, everolimus (RAD001) and temsirolimus (CCI-779) have been approved by the Food and Drug Administration to treat advanced renal cell calcinoma,[3,4] and clinical trials for mTORC1 inhibitors are ongoing for several types of cancer.[5]

Colorectal cancer is one of the leading causes of cancer deaths. We previously showed that RAD001 suppressed intestinal tumorigenesis in adenomatous polyposis coli (*Apc*$^{\Delta 716}$) mice, and extended their survival significantly, suggesting that mTORC1 inhibition could be a useful colon cancer therapy.[6] Although the study showed that Wnt/β-catenin signaling contributed to mTORC1 activation by increasing the mTOR protein level, it was unclear whether Wnt/β-catenin signaling was sufficient for mTORC1 activation in the intestinal polyps of *Apc*$^{\Delta 716}$ mice.

The c-Jun N-terminal kinase (JNK) is a serine/threonine kinase that affects proliferation, differentiation, survival, and migration.[7] The JNK signaling is activated in human colon cancer tissues,[8] and has been implicated in some other types of cancer as well. Namely, *Jnk1* knockout reduced hepatocellular carcinogenesis induced by diethylnitrosamine,[9] as well as gastric cancer formation induced by N-methyl-N-nitrosourea.[10] Furthermore, the number and size of polyps in *Apc*^{min} mouse intestines were reduced by introduction of a c-Jun mutation carrying alanine substitutions at the JNK phosphorylation sites.[11] Interestingly, some of the phenotypes of *Jnk1* knockout mice are similar to those of mutants in S6K, an mTORC1 substrate. For example, mutant mice for either gene show decreased body weight and reduced levels of

Abbreviations used in this paper: Apc, adenomatous polyposis coli; mTOR, mammalian target of rapamycin; JNK, c-Jun-NH_2 terminal kinase; shRNA, short hairpin RNA; siRNA, small interfering RNA; WT, wild-type.

0016-5085/$36.00
doi:10.1053/j.gastro.2011.02.007

circulating insulin.[12–14] Here we show that activation of JNK signaling induces mTORC1 signaling, and that inhibition of JNK signaling reduces intestinal tumorigenesis. We also show that JNK can directly activate mTORC1 through phosphorylation of Raptor.

Materials and Methods

Animals and Drug Treatments

The construction of $Apc^{\Delta 716}$ knockout mice was described previously.[15] Male and female $Apc^{\Delta 716}$ mice at 8 weeks of age were gavaged with SP600125 (50 mg/kg/day) (Sigma Chemical Co, St. Louis, MO) or the vehicle (0.5% hydroxyethyl cellulose) for 4 weeks. RAD001 (everolimus) was provided by Novartis Institutes for BioMedical Research (Basel, Switzerland). A total of 10 mg/kg/day of RAD001 was administered for 2 weeks as microemulsion containing 2% (wt/wt) RAD001 diluted in distilled deionized water by oral gavage. All animal experiments were performed according to the protocols approved by the Animal Care and Use Committee of Kyoto University.

Histologic Analysis and Immunohistochemistry

Tissues were fixed in 10% formalin-phosphate-buffered saline (PBS) for staining p-c-Jun or in 4% paraformaldehyde-PBS for staining p-S6, β-catenin, and proliferin. Paraffin-embedded samples were sectioned at 4-μm thickness and stained with H&E or subjected to immunohistochemistry. Sections were stained with antibodies against β-catenin (Sigma), p-S6, p-c-Jun (Cell Signaling Technology, Danvers, MA), or proliferin (R&D Systems, Minneapolis, MN), with prior antigen retrieval by microwave in sodium citrate buffer (pH 6.0). After the incubation with primary antibodies, sections were incubated with biotinylated secondary antibodies (Vector Laboratories, Burlingame, CA). The peroxidase activity was detected with Vectorstain Elite kit (Vector Laboratories) and DAB Substrate kit (Vector Laboratories).

Polyp Scoring

Intestinal polyps were counted as described previously.[15] Briefly, the small and large intestines were excised, washed with ice-cold PBS, and opened longitudinally. After fixation with 4% paraformaldehyde-PBS, the number and size of polyps were scored under a dissection microscope.

Cell Cultures and Transfection

We obtained human colon cancer cell lines SW480 and HT29 from M. Tsujii (Osaka University, Osaka, Japan). RKO cells were purchased from American Type Culture Collection. Cells were cultured in Dulbecco's modified Eagle medium supplemented with 10% fetal bovine serum (Biowest, Nuaille, France). For starvation, the cells were cultured in serum-free Dulbecco's modified Eagle medium or in Dulbecco's PBS containing 45 mmol/L glucose. SP600125 (Sigma) and anisomycin (Sigma) were dissolved in dimethyl sulfoxide, and then used to treat the cells at concentrations of 50 μmol/L and 1 μg/mL, respectively. Expression vectors were transfected using Lipofectamine 2000 (Invitrogen, Carlsbad, CA). Transfection with siRNA was performed using Lipofectamine 2000 (Invitrogen), adjusting the final RNA concentration to 40 nmol/L. The small interfering RNAs (siRNAs) were designed to target human *APC* (Verma et al[16]; Dharmacon, Lafayette, CO) and c-Jun (5′-GGAAGCUGGAGAGAAUCGCdTdT-3′; Hayashi Kasei, Osaka, Japan). Scramble RNA was used as a control (Hokkaido System Science, Sapporo, Japan).

Western Blot Analysis

Western blot analysis was performed as described previously.[6] Whole lysates of the intestinal polyps were prepared from 2–3 polyps per sample. The lysates were applied to sodium dodecyl sulfate-polyacrylamide gel electrophoresis, transferred to a polyvinylidene fluoride microporous membrane (Millipore, Billerica, MA), and immunoblotted with antibodies for cyclin E, c-myc tag (Santa Cruz, Santa Cruz, CA), β-catenin, β-actin (Sigma), p-JNK1/2, p-c-Jun, p-S6, S6, p-S6 kinase, S6 kinase, p-4EBP1, 4EBP1, p-Akt (Cell Signaling Technology), proliferin (R&D Systems), osteopontin (IBL, Fujioka, Japan), MMP7 (Merck, Darmstadt, Germany), c-Myc (Millipore), or His-tag (MBL, Nagoya, Japan). Immuno-specific bands were detected by chemiluminescence using Immobilon Western Chemiluminescent Horseradish-Peroxidase Substrate (Millipore).

Reverse-Transcription Polymerase Chain Reaction Analysis

Total RNA from cultured cells or mouse tissues was extracted using TRI Reagent (Sigma), according to the manufacturer's protocol. Each RNA sample (4 μg) was reverse-transcribed and subjected to polymerase chain reaction under the following conditions: cyclin E: denaturation at 94°C for 45 seconds, annealing at 60°C for 45 seconds, and extension at 72°C for 1 minute, for 28 cycles; proliferin and osteopontin: denaturation at 94°C for 30 seconds, annealing at 55°C for 45 seconds, and extension at 72°C for 1 minute, for 28 cycles. The primers for human cyclin E were as follows: 5′-AATCGACAGGACGGCGAGGGAC- 3′ (forward) and 5′-GGCAGTCAACATCCAGGACACA-3′ (reverse). The primers for mouse proliferin were as follows: 5′-TGTGTGCAATGAGGAATGGT-3′ (forward) and 5′-AACCAGGCAGGGTTCTTCTT-3′ (reverse). The primers for mouse osteopontin were as follows: 5′-AAGCTTCCATGGGAATTGGAGTGATTTGCTTTTGCCTC-3′ (forward) and 5′-GGATCCTTAATTGACCTCAGAAGATGCACTATCTAA-3′ (reverse). The control reverse-transcription polymerase chain reaction for glyceraldehyde-3-phosphate dehydrogenase was performed as internal controls.

Statistical Analysis

Data were analyzed by the Student *t* test and are expressed as means ± standard deviation. *P* values less than .05 were considered significant.

See the Supplementary Materials and Methods section and Supplementary Table 1 for details of vector construction and site-directed mutagenesis, lentiviral short hairpin RNA (shRNA) cloning and infection, recombinant protein, kinase assay, and microarray.

Results

Wnt Signaling Is Insufficient for mTORC1 Activation in Intestinal Polyps

We previously showed that the known upstream effectors of mTORC1, namely the phosphatidylinositol-3K/Akt pathway, MAPK/Erk kinase (Mek)/Extracellular signal-regulated kinase (Erk) pathway, and energy status were not directly involved in mTORC1 pathway activation in the intestinal polyps of $Apc^{\Delta 716}$ mice,[6] suggesting an alternative pathway(s) that activates mTORC1 signaling in the polyp adenomas. Because formation of the intestinal polyps in $Apc^{\Delta 716}$ mice is initiated by activation of Wnt signaling through homozygous loss of *Apc*,[15] we first determined whether Wnt signaling activation was sufficient for mTORC1 activation in the polyps. We stained for β-catenin and for the phosphorylated form of ribosomal S6 protein, a substrate of p70S6K downstream of mTORC1. We found strong β-catenin staining in the cytoplasm and nuclei of adenoma epithelial cells, including those in nascent polyps, but not in normal intestinal epithelial cells, indicating Wnt signal activation specifically in the tumor epithelium (Figure 1*A*). On the other hand, S6 was phosphorylated in the adenoma epithelium of only large polyps (>1.0 mm diameter), but not in the nascent ones (<0.5 mm) (Figure 1*B*). These results indicate that Wnt signaling induced by the loss of *Apc* gene does not lead to instant activation of mTORC1 signaling. Consistently, siRNA-mediated knockdown of *APC* in RKO cells, a colon cancer cell line in which Wnt signaling was not activated, failed to increase the phosphorylation level of S6K (Supplementary Figure 1*A*), despite that it increased the levels of β-catenin protein and mRNAs for Wnt target genes *cyclin D1* (*CCND1*) and *c-myc* (*MYC*) (Supplementary Figure 1*A* and *B*). These results indicate that Wnt signaling activation alone is insufficient for the mTORC1 signaling activation.

Tumor Size-Dependent Activation of JNK and mTORC1 Signaling in Intestinal Polyps

Because JNK was implicated in both mTORC1 signaling and intestinal tumorigenesis as described earlier, we next assessed the activation status of JNK signaling in the polyps of $Apc^{\Delta 716}$ mice by immunostaining for phospho-c-Jun (p-c-Jun), a representative substrate of JNK. Interestingly, c-Jun was phosphorylated in the adenoma cell nuclei of large polyps, but not in those of nascent ones (Figure 1*C*), reminiscent of the staining pattern for p-S6 (Figure 1*B*). Consistently, a Western blot analysis showed polyp size-dependent phosphorylation of JNK and c-Jun, as well as of S6 and 4EBP1, the downstream effectors of mTORC1 (Figure 1*D*). These results suggest that JNK signaling may be associated with the mTORC1 activation in intestinal tumors. To determine whether mTORC1 signaling was affected by JNK signaling, we treated $Apc^{\Delta 716}$ mice with the JNK inhibitor SP600125. Dosing with SP600125 markedly reduced the phosphorylation levels of S6K and S6, as well as those of JNK and c-Jun in the polyps as compared with the vehicle control (Figure 1*E* and *F*). These results indicate that activation of JNK is necessary for the mTORC1 signaling activation in the polyps of $Apc^{\Delta 716}$ mice.

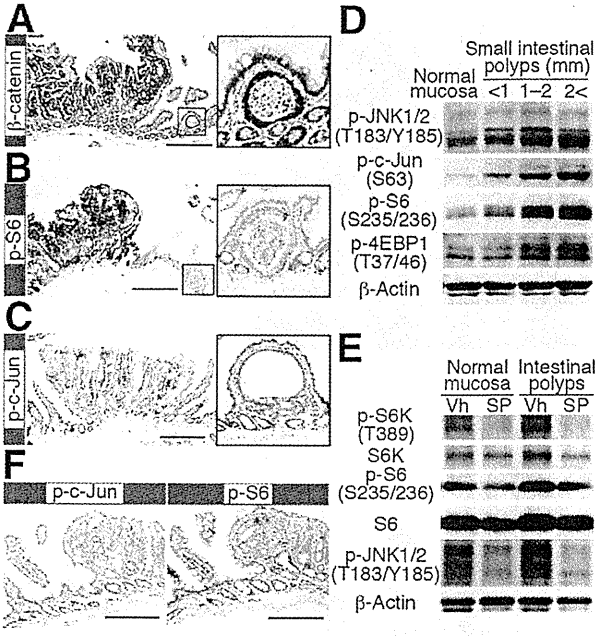

Figure 1. Activation of JNK and mTORC1 signaling in $Apc^{\Delta 716}$ mouse polyps. (*A–C*) Immunostaining for (*A*) β-catenin, (*B*) p-S6, and (*C*) p-c-Jun in intestinal polyps. (*D*) Western blot analysis for JNK and mTORC1 signaling in normal ileal mucosa and polyps of indicated sizes in $Apc^{\Delta 716}$ mice. Increased phosphorylation levels of JNK and c-Jun indicate JNK signaling, whereas those of S6 and 4EBP1 indicate mTORC1 activation. (*E*) Western blot analysis of mTORC1 signaling in intestinal polyps of SP600125-treated $Apc^{\Delta 716}$ mice. Vehicle (VH) or JNK inhibitor SP600125 (SP; at 50 mg/kg) was given for 2 weeks. (*F*) Immunostaining of p-c-Jun (left) and p-S6 (right) in intestinal polyps in SP600125-treated $Apc^{\Delta 716}$ mice. Bars: *A–C*, 500 μm; and *F*, 200 μm. Insets in *A–C* show subfields at 4-fold higher magnification.

Treatment With a JNK Inhibitor Blocks the Polyp Expansion in $Apc^{\Delta 716}$ Mice

Dosing $Apc^{\Delta 716}$ mice with the mTORC1 inhibitor RAD001 suppressed formation of intestinal tumors, especially those in the large size class (>1.5 mm).[6] We therefore hypothesized that treatment with JNK inhibitors might

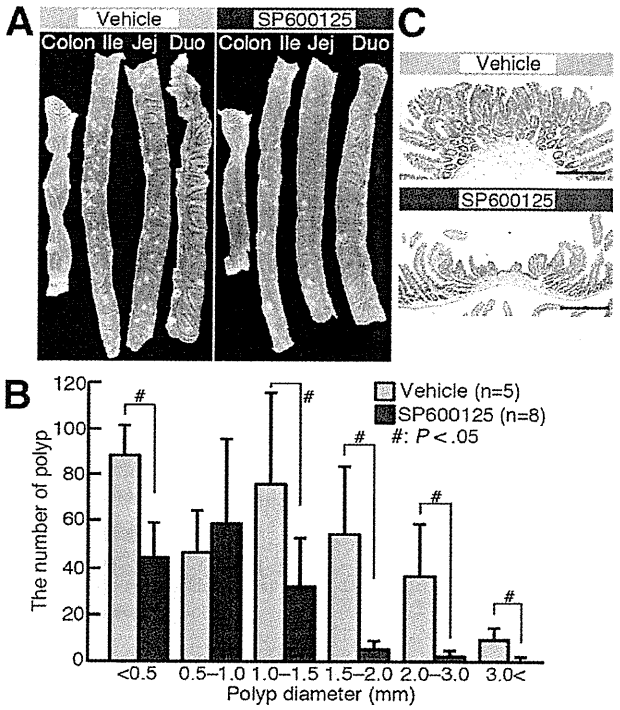

Figure 2. SP600125 suppresses polyp formation in $Apc^{\Delta 716}$ mice. (*A*) Gross appearance of intestinal polyps in $Apc^{\Delta 716}$ mice treated with vehicle or SP600125 at 50 mg/kg for 4 weeks. DUO, duodenum; JEJ, jejunum; ILE, ileum. (*B*) Size distribution of intestinal polyps in $Apc^{\Delta 716}$ mice treated with SP600125. (*C*) H&E-staining of polyps in vehicle- (left panel) or SP600125-treated (right panel) $Apc^{\Delta 716}$ mice. Bar, 500 μm.

have similar effects to those by inhibition of mTORC1. To test the possibility, we dosed $Apc^{\Delta 716}$ mice with the JNK inhibitor SP600125 (50 mg/kg) for 4 weeks. It significantly reduced the total number of intestinal polyps in $Apc^{\Delta 716}$ mice (mean ± standard deviation, 143.5 ± 69.4), compared with the vehicle control (mean ± standard deviation, 311.0 ± 68.8) (Figure 2*A* and *B*). Notably, the number of large polyps (>1.5 mm) was reduced dramatically in the SP600125-treated $Apc^{\Delta 716}$ mice (7.5 vs 99.8 [vehicle]) (Figure 2*B*). Interestingly, polyps in the SP600125-treated mouse showed a collapsed morphology at the top (Figure 2*C* and *D*), similar to those in the mTORC1 inhibitor-treated mice.[6] These results suggest that JNK signaling plays a key role in the intestinal tumorigenesis in $Apc^{\Delta 716}$ mice, upstream of the mTORC1 signaling.

JNK Activates mTORC1 Signaling Directly

Suppression of mTORC1 activation and of polyp formation by SP600125 in $Apc^{\Delta 716}$ mice suggests that JNK lies upstream of mTORC1 in vivo. To determine the role of JNK signaling in mTORC1, we treated colon cancer cell lines with JNK activator anisomycin or its inhibitor SP600125. As shown in Figure 3*A*, anisomycin increased the phosphorylation level of S6K in SW480 and HT29 cells, compared with the vehicle control (Figure 3*A*). On the other hand, SP600125 significantly reduced the phosphorylation of S6K in SW480 and HT29 cells (Figure 3*B*). Consistently, overexpression of JNK1, but not the kinase-dead JNK (K55R), increased the phosphorylation of both S6K and S6 protein (Supplementary Figure 2*A*), although neither of them affected the phosphorylation of Akt at Ser473, a residue implicated in Akt activation by mTORC2 (Supplementary Figure 2*A*). Likewise, shRNA-mediated knockdown of JNK decreased the phosphorylation level of S6K compared with the scramble RNA (Supplementary Figure 2*B*). These results suggest that the activation of JNK signaling is both necessary and sufficient for mTORC1 activation in colon cancer cells. We then investigated the mechanism by which JNK signaling activated mTORC1. We first tested whether JNK acted upstream or downstream of Rheb. Rheb is a small guanosine triphosphatase that can directly activate mTORC1.[17,18] As shown in Figure 3*C*, Rheb-induced S6K phosphorylation at Thr389 in SW480 cells was significantly inhibited by treatment with SP600125 (Figure 3*C*). Consistently, JNK knockdown by shRNA against JNK1/2 significantly reduced Rheb-induced S6K phosphorylation in SW480 cells (Figure 3*D*). These results suggest that JNK signaling affects mTORC1 at the downstream of Rheb.

JNK Up-Regulates mTORC1 Kinase Activity In Vitro

We then tested whether JNK could directly stimulate the mTORC1 kinase activity in vitro, using the mTOR immune complex prepared from 3-[(3-cholamidopropyl) dimethylammonio]-1-propanesulfonate (CHAPS)-solubilized cell lysates. As shown in Figure 3*E*, addition of the recombinant JNK1 significantly enhanced the mTORC1 kinase activity as determined by phosphorylation of the substrate 4EBP1 (Figure 3*E*). This enhancement was inhibited by RAD001, confirming the mTORC1-mediated phosphorylation of 4EBP1 (Figure 3*E*). Furthermore, the kinase-dead JNK1 showed significantly reduced mTORC1 activation compared with the wild-type JNK1 (Figure 3*F*), suggesting an essential role of the kinase activity in JNK1-mediated mTORC1 activation. The weak but significant activity of the kinase-dead JNK1 may be owing to co-purification of some proteins from the Sf9 insect cells that can activate mTORC1 in vitro, or to a kinase-independent function of JNK1, which remains to be investigated. Taken together, these results indicate that JNK can directly stimulate the mTORC1 kinase activity in vitro.

JNK Stimulates mTORC1 Through Phosphorylation of Raptor at Ser 863

Because JNK is a proline-directed serine/threonine kinase,[19] we hypothesized that JNK might activate mTORC1 through phosphorylation of an mTORC1 component at serine or threonine residues preceding proline. We searched for such sites in mTORC1 using PhosphoSitePlus (http://www.phosphosite.org/homeAction.do), and found 3 candidate residues (serines 567, 1859,

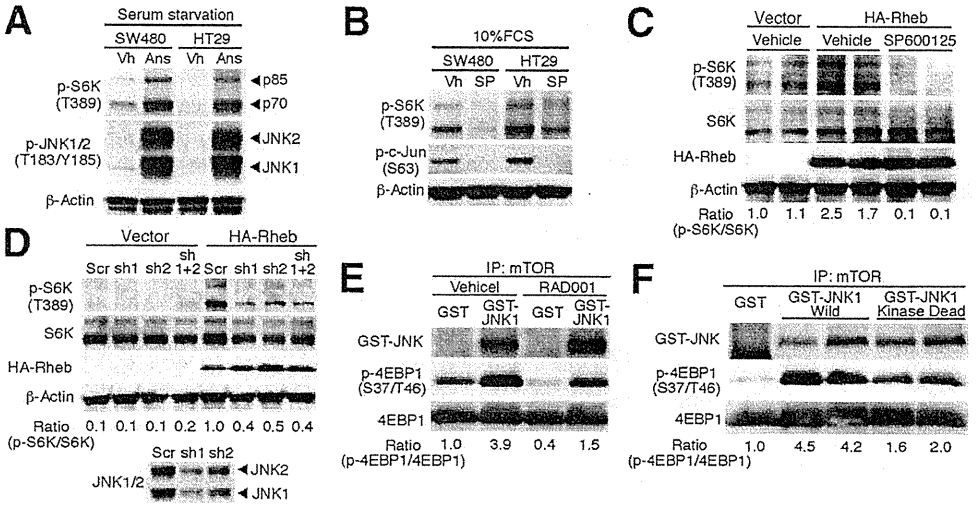

Figure 3. JNK signaling stimulates mTORC1 signaling. (*A*) Activation of JNK signaling stimulates mTORC1 signaling. Western blot analysis of p-S6K in colon cancer cell lines treated with JNK activator anisomycin (ANS; at 1 μg/mL) or vehicle control (VH) for 30 minutes. β-actin is shown as a loading control. (*B*) Inhibition of JNK signaling blocks mTORC1 signaling. Western blot analysis of p-S6K in colon cancer cell lines treated with SP600125 (SP; at 50 μmol/L) or vehicle (VH) for 6 hours. (*C*) SW480 cells transfected with HA-tagged ras homolog enriched in brain (Rheb) or vector control were starved in Dulbecco's PBS and treated with SP600125 (at 50 μmol/L) or vehicle for 30 minutes. (*D*) SW480 cells stably infected with shRNAs against JNK1/2 (sh1) or (sh2), either alone or in combination, or with scramble RNA (SCR). Cells were transfected with HA-Rheb or vector control, and starved for 30 minutes in D-PBS. Bottom panel shows successful knockdown of JNK1/2 by shRNA. (*E*) JNK activates mTORC1 in vitro. In vitro kinase assays were performed for mTORC1 with 4EBP1 as a substrate. mTORC1 was prepared from 293 cells treated with or without RAD001 by immunoprecipitation with an mTOR antibody. The immunoprecipitates were incubated with glutathione S-transferase (GST)-JNK or GST, and adenosine triphosphate for 20 minutes. 4EBP1 was added with or without 20 nmol/L RAD001, and the mixtures were incubated further for 30 minutes. Samples were subjected to Western blot analysis. (*F*) JNK kinase activity is required for activating mTORC1. mTORC1 in vitro kinase assays were performed with 4EBP1 as substrate. mTORC1 was prepared from 293 cells by immunoprecipitation with the mTOR antibody. The immunoprecipitates were incubated with GST-JNK (WILD) or GST-K55R, and adenosine triphosphate for 20 minutes. 4EBP1 was added and the mixtures were incubated further for 30 minutes. Samples were subjected to Western blot analysis.

and 1863) in mTOR itself and 2 candidate residues (serines 863 and 877) in Raptor, an essential component of mTORC1 (Supplementary Figure 3*A*). To determine whether JNK could phosphorylate mTOR or Raptor directly, we overexpressed myc-mTOR or myc-Raptor in 293T cells, and immunoprecipitated them from the cell lysate with an anti-myc antibody. Immune complex kinase assays showed that the recombinant JNK phosphorylated Raptor, but not mTOR in vitro (Figure 4*A*). To identify JNK phosphorylation sites in Raptor, we constructed mutant Raptor constructs with serine 863 or 877 substituted with alanine (S863A or S877A). As a control, we substituted the 3 serine phosphorylation sites for p90 ribosomal protein s6 kinase (RSK) at 719, 721, and 722 with alanine (AAA mutant).[20] In vitro kinase assays showed that the S863A mutation greatly reduced phosphorylation of Raptor by JNK, although it phosphorylated wild-type (WT) Raptor as well as the AAA and S877A mutants (Figure 4*B*). In vitro kinase assays using a recombinant Raptor fragment confirmed direct phosphorylation of Raptor by JNK at serine 863 (Figure 4*C*). To determine the role of Raptor phosphorylation at serine 863 in mTORC1 activation by JNK, we next performed kinase assays using myc-Raptor or myc-Raptor S863A overexpressed in SW480 cells. As shown in Figure 4*D*, JNK failed to enhance the kinase activity of mTORC1 (determined by 4EBP1 phosphorylation) containing myc-Raptor S863A, suggesting that phosphorylation of Raptor at serine 863 is essential for the JNK-mediated mTORC1 activation. Phosphorylation of Raptor at serine 863 was indeed increased in the intestinal polyps of $Apc^{\Delta 716}$ mice compared with normal mucosa (Supplementary Figure 3*B*). These results indicate that JNK stimulates mTORC1 signaling through phosphorylation of Raptor at serine 863, and thereby enhances intestinal polyp expansion in $Apc^{\Delta 716}$ mice.

JNK Up-Regulates Cyclin E in Intestinal Tumor Cells Through Two Distinct Mechanisms

We previously showed that the cyclin E protein level was reduced significantly in the intestinal polyps of $Apc^{\Delta 716}$ mice treated with RAD001.[6] Consistent with the role of JNK in mTORC1 activation in intestinal tumors, stimulation of the serum-starved HT29 cells with JNK activator anisomycin or 10% fetal calf serum (positive control) increased the level of cyclin E protein (Figure 5*A*), which was inhibited by treatment with RAD001 (Figure 5*A*). Importantly, anisomycin failed to enhance cyclin E protein level in JNK-knockdown HT29 cells

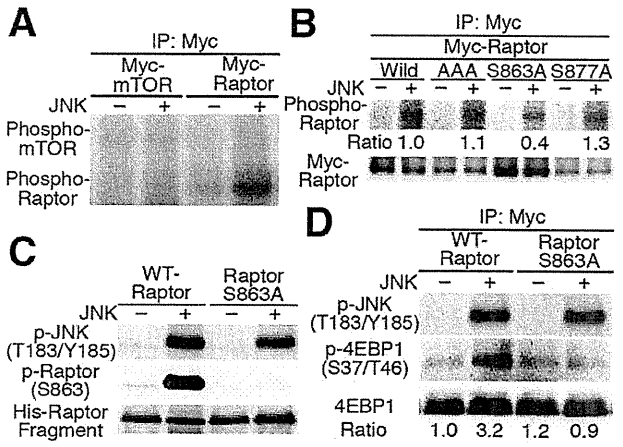

Figure 4. JNK directly activates mTORC1 through Raptor phosphorylation. (*A*) JNK phosphorylates Raptor, but not mTOR. In vitro kinase assays for JNK with immunoprecipitated mTOR or Raptor as substrate. mTOR or Raptor was prepared from 293T cells overexpressing myc-mTOR or myc-Raptor by immunoprecipitation with a myc antibody. The immunoprecipitates were incubated with or without recombinant glutathione S-transferase (GST)–JNK. [γ-^{32}P]Adenosine triphosphate was added and the mixtures were incubated for 30 minutes. Phosphorylation was detected by autoradiography. (*B*) JNK phosphorylates Raptor at serine 863. In vitro kinase assays for JNK using Raptor mutants as substrate. The Raptor protein was immunoprecipitated with myc antibody from 293T cells overexpressing myc-tagged WT or mutant Raptor. The immunoprecipitates were incubated with or without recombinant GST-JNK. [γ-^{32}P]Adenosine triphosphate was added and the mixtures were incubated for 30 minutes. Phosphorylation was detected by autoradiography. (*C*) In vitro kinase assay for JNK using recombinant Raptor fragment (amino acids 668~938) as substrate. A His-tagged recombinant Raptor protein was incubated with or without recombinant GST-JNK. Adenosine triphosphate was added and incubated for 30 minutes. Phosphorylation of Raptor at serine 863 was detected with p-Raptor (S863) antibody. Recombinant GST-JNK and His-tagged Raptor were detected by anti–p-JNK antibody and anti–His-tag antibodies, respectively. (*D*) Serine 863 of Raptor is important for mTORC1 activation. In vitro kinase activity was assayed for mTORC1 using 4EBP1 as substrate. mTORC1 containing WT- or S863A-Raptor was prepared from SW480 cells overexpressing myc-WT– or myc-S863A–Raptor by immunoprecipitation with myc-antibody. The immunoprecipitates were incubated with recombinant JNK and adenosine triphosphate for 20 minutes, and then 4EBP1 was added. The mixtures were incubated for an additional 30 minutes and then subjected to Western blot analysis.

(Figure 5*A*). These results suggested that increased cyclin E protein level was caused by JNK activation through mTORC1 signaling. We then tested whether JNK signaling would affect the cyclin E mRNA level. Treatment with anisomycin, as well as with 10% fetal calf serum, significantly increased the level in HT29 cells (Figure 5*B*). However, RAD001 did not affect the cyclin mRNA induction by anisomycin or fetal calf serum. An siRNA against c-Jun also reduced the level significantly in HT29 cells compared with a scramble RNA-treated control (Figure 5*C*). These results suggest that JNK activation in intestinal tumors enhances cyclin E expression through 2 mechanisms: by increasing the mRNA level via activation of c-Jun, a RAD001-insensitive pathway, and through increasing the protein level via mTORC1 activation, a RAD001-sensitive pathway.

JNK/mTORC1 Signaling Increases the Levels of Proliferin and Osteopontin in Intestinal Polyps of Apc$^{\Delta 716}$ *Mice*

The earlier results suggest that JNK activation can contribute to intestinal tumor expansion by 2 mechanisms. Because intestinal tumorigenesis is induced by Wnt signaling, we have determined whether JNK affects expression of Wnt target genes in a similar manner. Target genes common to Wnt and JNK pathway include *c-Myc*, *Mmp7*, *Cd44*, *osteopontin*, *Wnt2*, and *proliferin*.[21–24] Microarray analysis showed an extremely high level of *proliferin* mRNA in the polyps compared with normal mucosa (>900-fold), whereas the mRNA levels for *Mmp7*, *c-Myc*, and *osteopontin* were increased moderately (>2-fold). On the other hand, *Cd44* expression was increased only slightly (>1.3-fold), and *Wnt2* expression was undetectable (Supplementary Table 1). Although the level of proliferin protein was increased in the intestinal polyps compared with normal mucosa, RAD001 treatment reduced it to that of normal mucosa (Supplementary Figure 4*A* and *B*). The protein levels of osteopontin, c-Myc, and Mmp7 also were increased in the polyps compared with normal mucosa. Although RAD001 markedly reduced the level of osteopontin, that of Mmp7 or c-Myc was not affected significantly (Supplementary Figure 4*C*). Notably, SP600125 significantly reduced the mRNA and protein levels of both proliferin and osteopontin in the

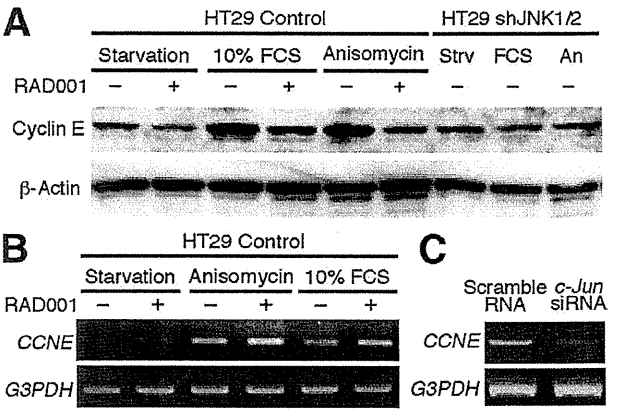

Figure 5. JNK signaling affects cyclin E at both protein and mRNA levels. (*A*) Western blot analysis for cyclin E protein level in HT29 cells treated with JNK activator anisomycin (1 μg/mL), or with anisomycin and mTORC1 inhibitor RAD001 (20 nmol/L) for 2 hours. The cyclin E level was not affected by serum or anisomycin stimulation in JNK1/2 knocked-down HT29 cell. (*B*) Reverse-transcription polymerase chain reaction analysis of cyclin E mRNA in HT29 cells. Starved cells were stimulated with anisomycin (1 μg/mL) or 10% fetal calf serum (FCS) for 1 hour in the presence or absence of 20 nmol/L RAD001. (*C*) Reverse-transcription polymerase chain reaction analysis of cyclin E mRNA in HT29 cells transfected with siRNA against *c-Jun* or with scramble RNA.

polyps (Supplementary Figure 4*D* and *F*), whereas RAD001 had no effect on their expression (Supplementary Figure 4*E*). These results suggest that JNK increases expression of not only cyclin E, but also proliferin and osteopontin in intestinal tumor cells. Because proliferin and osteopontin are implicated in angiogenesis[25,26] and metastasis,[27] respectively, JNK may enhance tumor formation by up-regulating these molecules.

Discussion

We showed earlier that mTORC1 signaling was activated constitutively in the intestinal polyps of $Apc^{\Delta 716}$ mice, and that intestinal tumorigenesis was suppressed significantly by treatment with the mTORC1 inhibitor RAD001, accompanied by reduced cyclin levels and inhibition of tumor angiogenesis.[6] We have shown here that JNK signaling stimulates intestinal tumorigenesis in $Apc^{\Delta 716}$ mice through activation of the mTORC1 signaling. Namely, Wnt signaling induced by loss of *Apc* is insufficient for mTORC1 signaling both in vivo and in vitro (Figure 1 and Supplementary Figure 1). We conclude that JNK plays an essential role in mTORC1 activation based on the following results. First, both JNK and mTORC1 showed tumor size-dependent activation (Figure 1*D*). Second, treatment with a JNK inhibitor blocked mTORC1 signaling and significantly reduced the number of large polyps (>1.5 mm diameter) in $Apc^{\Delta 716}$ mice (Figures 1*E* and 2), similar to treatment with an mTORC1 inhibitor. Third, studies using colon cancer cell lines showed JNK mediated mTORC1 activation whereas JNK inhibition suppressed it (Figure 3*A* and *B*).

JNK is known to be activated by stresses such as ultraviolet irradiation and hydrogen peroxide treatment.[28,29] The intestines are exposed to bacteria, mechanical stresses, and digestive juices that can activate JNK signaling (Supplementary Figure 5*A*). We have shown here that JNK promotes mTORC1 activation through direct phosphorylation of Raptor at serine 863. Although it remains unclear how mTORC1 activity is regulated by phosphorylation of Raptor, several groups recently have reported the roles of Raptor phosphorylation in mTORC1 activation. Namely, RSK stimulated by mitogen-activated protein kinase signaling phosphorylates Raptor at serines 719, 721, and 722, which increases the mTORC1 activity.[20] Raptor is phosphorylated also by mTOR at serine 863, which stimulates the mTORC1 activity.[30,31] Other links between mTORC1 and JNK also have been reported. For example, JNK can enhance the S6K kinase activity through phosphorylation of S6K at serine 411;[32] and mTORC1 signaling can stimulate JNK signaling indirectly.[33] These multiple mechanisms may cooperate to amplify the signal.

JNK signaling is frequently activated in colorectal cancer,[8,34] and has been implicated in cell proliferation rather than cell death in the intestines.[35,36] Studies using mouse models have shown that JNK signaling promotes normal epithelial cell proliferation and intestinal tumorigenesis.[11,37,38] Although it was reported that $Jnk1^{-/-}$ mice developed spontaneous intestinal tumors (<1 polyp per animal),[39] other groups did not find any tumors in the intestines of $Jnk1^{-/-}$ mice.[40] Colon cancer induction by a chemical carcinogen was not affected either by *Jnk1* or *c-Jun* gene disruption in the intestinal epithelium.[40]

Our present results suggest that the JNK/mTORC1 signaling axis enhances intestinal tumorigenesis in $Apc^{\Delta 716}$ mice by promoting proliferation of tumor cells initiated by Wnt signaling. Activation of mTORC1 signaling by JNK may help increase translation of some mRNAs involved in tumor cell proliferation. We have found that protein levels of cyclin E, proliferin, and osteopontin were reduced by RAD001 (Figure 5 and Supplementary Figure 4), suggesting a role of mTORC1 in the biosynthesis of these proteins. Interestingly, the levels of mRNA for these molecules were reduced significantly by knockdown of c-Jun or by SP600125 (Figure 5 and Supplementary Figure 4*E*), indicating that JNK stimulates their transcription through c-Jun. Thus, JNK may induce expression of some proteins involved in tumor growth by 2 mechanisms: by promoting transcription via c-Jun phosphorylation, and by enhancing mRNA translation via mTORC1 activation (Supplementary Figure 5*B*).

Supplementary Material

Note: To access the supplementary material accompanying this article, visit the online version of *Gastroenterology* at www.gastrojournal.org, and at doi: 10.1053/j.gastro.2011.02.007.

References

1. Guertin DA, Sabatini DM. Defining the role of mTOR in cancer. Cancer Cell 2007;12:9–22.
2. Laplante M, Sabatini DM. mTOR signaling at a glance. J Cell Sci 2009;122:3589–3594.
3. Hudes G, Carducci M, Tomczak P, et al. Temsirolimus, interferon alfa, or both for advanced renal-cell carcinoma. N Engl J Med 2007;356:2271–2281.
4. Mother RJ, Scudder B, Oudard S, et al. Efficacy of everolimus in advanced renal cell carcinoma: a double-blind, randomised, placebo-controlled phase III trial. Lancet 2008;372:449–456.
5. Easton JB, Houghton PJ. mTOR and cancer therapy. Oncogene 2006;25:6436–6446.
6. Fujishita T, Aoki K, Lane HA, et al. Inhibition of the mTORC1 pathway suppresses intestinal polyp formation and reduces mortality in $Apc^{\Delta 716}$ mice. Proc Natl Acad Sci U S A 2008;105:13544–13549.
7. Wagner EF, Nebrada AR. Signal integration by JNK and p38 MAPK pathways in cancer development. Nat Rev Cancer 2009;9:537–549.
8. Licato LL, Brenner DA. Analysis of signaling protein kinases in human colon or colorectal carcinomas. Dig Dis Sci 1998;43:1454–1464.
9. Sakurai T, Maeda S, Chang L, et al. Loss of hepatic NF-κB activity enhances chemical hepatocarcinogenesis through sustained c-Jun N-terminal kinase 1 activation. Proc Natl Acad Sci U S A 2006;103:10544–10551.

10. Shibata W, Maeda S, Hikiba Y, et al. c-Jun NH2-terminal kinase 1 is a critical regulator for the development of gastric cancer in mice. Cancer Res 2008;68:5031–5039.
11. Nateri AS, Spencer-Dene B, Behrens A. Interaction of phosphorylated c-Jun with TCF4 regulates intestinal cancer development. Nature 2005;437:281–285.
12. Shima H, Pende M, Chen Y, et al. Disruption of the p70(s6k)/p85(s6k) gene reveals a small mouse phenotype and a new functional S6 kinase. EMBO J 1998;17:6649–6659.
13. Hirosumi J, Tuncman G, Chang L, et al. A central role for JNK in obesity and insulin resistance. Nature 2002;420:333–336.
14. Belgardt BF, Mauer J, Wunderlich FT, et al. Hypothalamic and pituitary c-Jun N-terminal kinase 1 signaling coordinately regulates glucose metabolism. Proc Natl Acad Sci U S A 2010;107:6028–6033.
15. Oshima M, Oshima H, Kitagawa K, et al. Loss of *Apc* heterozygosity and abnormal tissue building in nascent intestinal polyps in mice carrying a truncated *Apc* gene. Proc Natl Acad Sci U S A 1995;92:4482–4486.
16. Verma UN, Surabhi RM, Schmaltieg A, et al. Small interfering RNAs directed against β-catenin inhibit the in vitro and in vivo growth of colon cancer cells. Clin Cancer Res 2003:9:1291–1300.
17. Inoki K, Li Y, Xu T, et al. Rheb GTPase is a direct target of TSC2 GAP activity and regulates mTOR signaling. Genes Dev 2003;17:1829–1834.
18. Long X, Lin Y, Ortiz-Vega S, et al. Rheb binds and regulates the mTOR kinase. Curr Biol 2005;15:702–713.
19. Cano E, Mahadevan LC. Parallel signal processing among mammalian MAPKs. Trends Biochem Sci 1995;20:117–122.
20. Carrière A, Cargnello M, Julien LA, et al. Oncogenic MAPK signaling stimulates mTORC1 activity by promoting RSK-mediated raptor phosphorylation. Curr Biol 2008;18:1269–1277.
21. Saadeddin A, Babaei-Jadidi R, Spencer-Dene B, et al. The links between transcription, β-catenin/JNK signaling, and carcinogenesis. Mol Cancer Res 2009;7:1189–1196.
22. Ziegler S, Röhrs S, Tickenbrock L, et al. Novel target genes of the Wnt pathway and statistical insights into Wnt target promoter regulation. FEBS J 2005;272:1600–1615.
23. Shaulian E, Karin M. AP-1 as a regulator of cell life and death. Nat Cell Biol 2002;4:E131–E136.
24. Groskopf JC, Linzer DI. Characterization of a delayed early serum response region. Mol Cell Biol 1994;14:6013–6020.
25. Jackson D, Volpert OV, Bouck N, et al. Stimulation and inhibition of angiogenesis by placental proliferin and proliferin-related protein. Science 1994;266:1581–1584.
26. Toft DJ, Rosenberg SB, Bergers G, et al. Reactivation of proliferin gene expression is associated with increased angiogenesis in a cell culture model of fibrosarcoma tumor progression. Proc Natl Acad Sci U S A 2001;98:13055–13059.
27. Irby RB, McCarthy SM, Yeatman TJ. Osteopontin regulates multiple functions contributing to human colon cancer development and progression. Clin Exp Metastasis 2004;21:515–523.
28. Johnson GL, Nakamura K. The c-jun kinase/stress-activated pathway: regulation, function and role in human disease. Biochim Biophys Acta 2007;1773:1341–1348.
29. Ruffels J, Griffin M, Dickenson JM. Activation of ERK1/2, JNK and PKB by hydrogen peroxide in human SH-SY5Y neuroblastoma cells: role of ERK1/2 in H_2O_2-induced cell death. Eur J Pharmacol 2004;483:163–173.
30. Wang L, Lawrence JC Jr, Sturgill TW, et al. Mammalian target of rapamycin complex 1 (mTORC1) activity is associated with phosphorylation of raptor by mTOR. J Biol Chem 2009;284:14693–14697.
31. Foster KG, Acosta-Jaquez HA, Romeo Y, et al. Regulation of mTOR complex 1 (mTORC1) by raptor Ser^{863} and multisite phosphorylation. J Biol Chem 2010;285:80–94.
32. Zhang Y, Dong Z, Nomura M, et al. Signal transduction pathways involved in phosphorylation and activation of p70S6K following exposure to UVA irradiation. J Biol Chem 2001;276:20913–20923.
33. Panaretakis T, Hjortsberg L, Tamm KP, et al. Interferon α induces nucleus-independent apoptosis by activating extracellular signal-regulated kinase 1/2 and c-Jun NH_2-terminal kinase downstream of phosphatidylinositol 3-kinase and mammalian target of rapamycin. Mol Biol Cell 2008;19:41–50.
34. Licato LL, Keku TO, Wurzelmann JI, et al. In vivo activation of mitogen-activated protein kinases in rat intestinal neoplasia. Gastroenterology 1997;113:1589–1598.
35. Weston CR, Wong A, Hall JP, et al. The c-Jun NH_2-terminal kinase is essential for epidermal growth factor expression during epidermal morphogenesis. Proc Natl Acad Sci U S A 2004;101:14114–14119.
36. Yamagata H, Matsuzaki K, Mori S, et al. Acceleration of Smad2 and Smad3 phosphorylation via c-Jun NH_2-terminal kinase during human colorectal carcinogenesis. Cancer Res 2005;65:157–165.
37. Sancho R, Nateri AS, de Vinuesa AG, et al. JNK signalling modulates intestinal homeostasis and tumourigenesis in mice. EMBO J 2009;28:1843–1854.
38. Endo H, Hosono K, Fujisawa T, et al. Involvement of JNK pathway in the promotion of the early stage of colorectal carcinogenesis under high-fat dietary conditions. Gut 2009;58:1637–1643.
39. Tong C, Yin Z, Song Z, et al. c-Jun NH2-terminal kinase 1 plays a critical role in intestinal homeostasis and tumor suppression. Am J Pathol 2007;171:297–303.
40. Hasselblatt P, Gresh L, Kudo H, et al. The role of the transcription factor AP-1 in colitis-associated and β-catenin-dependent intestinal tumorigenesis in mice. Oncogene 2008;27:6102–6109.

Received October 10, 2010. Accepted February 1, 2011.

Reprint requests

Address requests for reprints to: Makoto M. Taketo, MD, PhD, Department of Pharmacology, Graduate School of Medicine, Kyoto University, Yoshida-Konoé-Cho, Sakyo-Ku, Kyoto 606-8501, Japan. e-mail: taketo@mfour.med.kyoto-u.ac.jp; fax: (81) 75-753-4402.

Acknowledgments

The authors thank P. M. McSheehy for RAD001; M. Oshima, T. Kitamura, M. Sonoshita, S. Arimura, F. Kakizaki, A. Deguchi, and K. Aoki for discussions; M. Tsujii for the SW480 cells; F. Tamanoi for HA-Rheb expression plasmid; and A. Matsunaga for microarray analysis. The authors also thank R. A. Weinberg for pLKO.1; D. Trono for psPAX2 and pMD2.G; and D. M. Sabatini for pLKO.1 scramble shRNA, myc–mammalian target of rapamycin, and myc-Raptor plasmids.

Current address of M.A.: Division of Molecular Pathology, Aichi Cancer Center Research Institute, 1-1, Kanokoden, Chikusa-Ku, Nagoya 464-8681, Japan.

M.A. and M.M.T. are co-senior authors.

Conflicts of Interest

The authors disclose no conflicts.

Funding

Supported by a Grant-in-Aid for Scientific Research from the Ministry of Education, Culture, Sports, Science and Technology of Japan (M.M.T.), and by a Grant-in-Aid for Cancer Research for the Third-Term Comprehensive 10-Year Strategy for Cancer Control from the Ministry of Health, Labour and Welfare of Japan (M.A.). T. F. is supported by the Global COE Program "Center for Frontier Medicine" by Ministry of Education, Culture, Sports, Science and Technology (MEXT), Japan. The experiments using radioisotopes were performed at the Radioisotope Research Center of Kyoto University.

Supplementary Materials and Methods

Vector Construction and Site-Directed Mutagenesis

The full-length, WT JNK1b1 complementary DNA (cDNA) was isolated by a polymerase chain reaction–based cloning technique from SW480 cells. The cDNA was inserted into myc-tag expression vector pCMV-Tag3B (Agilent Technologies, Santa Clara, CA). Site-directed mutagenesis for K55R was performed using the QuikChange site-directed mutagenesis kit (Agilent Technologies) with the following oligomers: forward: 5′-GAAAGAAATGTTGCAATCA**g**GAAGCTAAGCCGACCATTT-3′, and reverse: 5′-AAATGGTCGGCTTAGCTTC**c**TGATTGCAACATTTCTTTC-3′. The lower case letters indicate the mutated bases encoding the adenosine triphosphate (ATP)-binding site of JNK. Expression plasmids for Myc-mTOR (Addgene #1861) and Myc-Raptor (Addgene #1859) were purchased from Addgene (Cambridge, MA). HA-Rheb expression plasmid was provided by F. Tamanoi (University of California Los Angeles, Los Angeles, CA). Site-directed mutagenesis for Raptor S863A, S877A, and AAA (S719A, S721A, S722A) was performed using PrimeSTAR MAX (Takara, Otsu, Japan) with the following oligomers: Raptor S863A forward: 5′-CCCGCCgcCCCCACCAACAAGGGCGTG-3′, and reverse: 5′-GGTGGGGgcGGCGGGGGCCGACTGCGT-3′. Raptor S877A forward: 5′-GGGGGGCgCCCCTCCGGCGTCCAGCA-3′, and reverse: 5′-GGAGGGGcGCCCCCCGCCTGGTGGAT-3′. Raptor AAA forward: 5′-GTgCTGTGgcCgCCTATGGAAACATCCGTG-3′, and reverse: 5′-AGGcGgcCACAGcACGAAGTCTGGGGGTGCA-3′. The lower cases indicate the mutated bases in Raptor to introduce the serine to alanine substitutions.

Lentiviral shRNA Cloning

Desalted oligonucleotides were annealed and cloned into pLKO.1 (Addgene #8453). The sequences of the oligonucleotides are as follows: JNK1/2 shRNA_1 sense, 5′-CCGGAAAGAATGTCCTACCTTCTTTCTCGAGAAAGAAGGTAGGACATTCTTTTTTTTG-3′; JNK1/2 shRNA_1 antisense, 5′-AATTCAAAAAAAAGAATGTCCTACCTTCTTTCTCGAGAAAGAAGGTAGGACATTCTTT-3′; JNK1 shRNA_2 sense, 5′-CCGGAAGCTCCACCACCAAAGATCCCTCGAGGGATCTTTGGTGGTGGAGCTTTTTTTG-3′; JNK1 shRNA_2 antisense, 5′-AATTCAAAAAAAGCTCCACCACCAAAGATCCCTCGAGGGATCTTTGGTGGTGGAGCTT-3′; JNK2 shRNA_2 sense, 5′-CCGGAAGGCACTGACCATATTGATCCTCGAGGATCAATATGGTCAGTGCCTTTTTTTG-3′; and JNK2 shRNA_2 antisense, and 5′-AATTCAAAAAAAGGCACTGACCATATTGATCCTCGAGGATCAATATGGTCAGTGCCTT-3′.

Lentivirus Production and Infection

For packaging, psPAX2 (Addgene #12260) and pMD2.G (Addgene #12259) were co-transfected with pLKO.1 containing the insert for scramble shRNA (Addgene plasmid #1864) or *JNK* shRNA of pLKO.1 into 293T cells by using Lipofectamine 2000 (Invitrogen). Virus-containing media were harvested 48 hours after transfection, and filtered through a sterile 0.45-micron filter (Millipore). Cells were infected with the virus stocks in the presence of 8 μg/mL polybrene (Millipore), and selected for puromycin resistance.

Recombinant JNK1 Protein

Glutathione S-transferase (GST)-tagged recombinant fusion proteins of WT- and K55R-human JNK1b1 were produced by a baculovirus expression system. JNK1b1 cDNA was inserted into pENTER 3C vector (Invitrogen). After recombination of JNK1 cDNA from pENTER 3C to pDEST 20 (Invitrogen), WT- or K55R-JNK1 pDEST 20 vector was transfected into Sf9 cells with Cellfectin reagent (Invitrogen). After amplification of the recombinant baculoviruses, fusion proteins were purified from the lysates of infected Sf9 cells using glutathione sepharose (GE Healthcare UK Ltd, Buckinghamshire, UK) from the recombinant baculovirus-infected Sf9 cells.

Kinase Assay for mTORC1

The mTORC1 complex was prepared from 293 cells. Cells were lysed in lysis buffer A (40 mmol/L HEPES [pH 7.4], 120 mmol/L NaCl, 1 mmol/L ethylenediaminetetraacetic acid [EDTA], 0.3% CHAPS, 10 mmol/L sodium pyrophosphate, 10 mmol/L NaF, and 1.5 mmol/L Na_3VO_4). The lysate was centrifuged at 14,000 × g for 5 minutes at 4°C, and the supernatant was incubated with anti-mTOR antibody (IBL) for 3 hours at 4°C, and incubated with protein G–agarose beads for 1 hour. The beads were washed 3 times with lysis buffer A, and once with kinase buffer A (25 mmol/L HEPES [pH 7.4], 50 mmol/L NaCl, 10 mmol/L $MnCl_2$, 10 mmol/L $MgCl_2$, and 50 mmol/L β-glycerophosphate). Kinase assays were performed at 30°C for 30 minutes in kinase buffer A with 200 μmol/L ATP, and 1 μg of 4EBP1 (Biomol, Plymouth Meeting, PA). Where indicated, the mixture was pretreated with 200 ng of recombinant JNK1 (Cell Signaling Technology), GST-WT-JNK1, or GST-K55R-JNK1 as described earlier. The reactions were terminated with 2× sample buffer. The phosphorylation level of 4EBP1 in samples was determined by Western blot analysis.

Kinase Assay for JNK using radioactive isotopes

Myc-tagged mTOR, WT-Raptor, Raptor S863A, Raptor S877A, and Raptor AAA proteins were overexpressed in 293T cells by transformation using Lipofectamine 2000. The cells were lysed in lysis buffer B (20 mmol/L Tris [pH 7.4], 150 mmol/L NaCl, 1 mmol/L EDTA, 1 mmol/L ethylene glycol bis(2-aminoethyl ether)-*N,N,N′,N′*-tetraacetic acid, 2% Triton-X100, 2.5 mmol/L sodium pyrophosphate, 1 mmol/L β-glycerophosphate, 1 mmol/L Na_3VO_4, and 1 μg/mL leupeptin). The lysate was

spun at 14,000 × g for 5 minutes at 4°C, and the supernatant was incubated with anti-myc antibody–conjugated agarose beads (Nacalai Tesque, Kyoto, Japan) overnight at 4°C. The beads were washed 3 times with lysis buffer B, and once with kinase buffer B (25 mmol/L Tris [pH 7.5], 5 mmol/L β-glycerophosphate, 2 mmol/L dithiothreitol, 0.1 mmol/L Na_3VO_4, and 10 mmol/L $MgCl_2$). Kinase assays were performed at 30°C for 30 minutes in kinase buffer B with 100 μmol/L cold ATP, and 200 kBq of [γ-^{32}P]ATP (PerkinElmer, Waltham, MA) with or without 200 ng/50 μL of JNK1 (Cell Signaling Technology). The reactions were terminated with 2× sample buffer. The samples were loaded on sodium dodecyl sulfate–polyacrylamide gel electrophoresis, and the dried gel was analyzed by a BAS 1800 II phosphoimager (Fujifilm, Tokyo, Japan).

Raptor Protein Fragment for JNK Kinase Assay

Bacterial expression vector for 6xHistidine-tagged WT- and S863A-Raptor (His-Raptor) were prepared by inserting human Raptor cDNA fragment (a.a. 668–938) into pET15b vector (Novagen, Madison, WI). BL21 *Escherichia coli* cells (BL21 Star [DE3]; Invitrogen) containing pET15b-His-Raptor were grown in LB medium with ampicillin and induced with 1 mmol/L isopropyl-β-D-thiogalactopyranoside for 4 hours at 30°C. The fusion proteins were purified with Ni-NTA His-Binds resins according to the manufacturer's protocol (Novagen). Kinase assays were performed at 30°C for 30 minutes in kinase buffer B with 200 μmol/L ATP, 1 μg of 6xHistidine-tagged WT- or S863A-Raptor protein, with or without 200 ng/50 μL of JNK1. The reactions were terminated with 2× sample buffer. The phosphorylation level of Raptor at Ser863 was determined by Western blot analysis with p-Raptor S863 antibody (Santa Cruz).

Supplementary Table 1. Gene Expression Profiles Analyzed by DNA Microarrays in Intestinal Polyps

	Gene	ID	Increased
1	*Proliferin*	NM_031191.1	906.82
2	*Il1rl1*	NM_001025602.2	125.51
3	*Phlda1*	NM_009344.3	122.82
4	*Atf1*	NM_007497.3	87.44
5	*Zfp62*	NM_009562.2	70.23
6	*Hbb-b2*	NM_016956.2	67.28
7	*Expi*	NM_007969.4	63.75
8	*Thbs1*	NM_011580.3	56.31
9	*Cfi*	NM_007686.2	55.64
10	*Foxq1*	NM_008239.4	50.75
11	*Me1*	NM_008615.2	46.94
12	*Pkd2*	NM_008861.3	46.06
13	*Gja1*	NM_010288.3	45.96
14	*Ctse*	NM_007799.3	45.49
15	*Gch1*	NM_008102.3	43.19
16	*Lmna*	NM_019390.2	41.71
17	*Rbp1*	NM_011254.5	41.61
18	*Hnrnpa1*	NM_010447.4	40.11
19	*Amd2*	NM_007444.3	36.23
20	*Hif1a*	NM_010431.2	35.61
21	*Morf4l2*	NM_001168225.1	35.31
22	*Kif5b*	NM_008448.3	33.85
23	*Rev3l*	NM_011264.3	33.77
24	*Ptpro*	NM_001164402.1	31.41
25	*Ube2e1*	NM_009455.3	30.94
26	*D030029J20Rik*	AW228840	30.55
27	*Mmp10*	NM_019471.2	29.52
28	*Marcks*	NM_008538.2	29.43
29	*Procr*	NM_011171.2	28.66
30	*Hars*	NM_008214.4	28.48
31	*Matr3*	NM_010771.6	27.82
32	*Dck*	NM_007832.4	27.48
33	*Cbx3*	NM_007624.3	27.26
34	*Tfdp1*	NM_009361.2	26.53
35	*A030003K02Rik*	AW124129	25.92
36	*Ctcf*	NM_181322.3	25.59
37	*Ranbp9*	NM_019930.2	25.48
38	*Hs3st1*	NM_010474.2	25.04
39	*Lrrc58*	NM_177093.3	24.35
40	*Il1rn*	NM_001039701.3	24.24
41	*Eftud2*	NM_011431.3	23.07
42	*Bub1*	NM_009772.2	23.06
43	*Pdgfra*	NM_011058.2	22.82
44	*Slc20a1*	NM_015747.2	22.79
45	*Hivep1*	NM_007772.2	22.66
46	*Cetn3*	NM_007684.3	22.26
47	*F3*	NM_010171.3	22.11
48	*Cxcl5*	NM_009141.2	22.10
49	*Amot*	NM_153319.2	21.95
50	*Strap*	NM_011499.3	21.60
51	*Ppic*	NM_008908.4	21.40
52	*Psmb5*	NM_011186.1	21.05
53	*Adh5*	NM_007410.2	20.62
54	*Fkbp1a*	NM_008019.2	20.41
55	*Kitl*	NM_013598.2	20.37
56	*H2afz*	NM_016750.2	20.30
57	*Syncrip*	NM_019666.2	20.20
58	*Robo1*	NM_019413.2	20.05
59	*Cxcr7*	NM_007722.3	19.90
60	*Galnt3*	NM_015736.2	19.51
61	*Atp6v1c1*	NM_025494.3	19.19

Supplementary Table 1. Continued

	Gene	ID	Increased
62	*Mcpt1*	NM_008570.1	18.77
63	*Snd1*	NM_019776.2	18.70
64	*Hells*	NM_008234.3	18.62
65	*T*	NM_009309.2	18.42
66	*Gpi1*	NM_008155.3	18.11
67	*Hmgb2*	NM_008252.3	18.09
68	*Smarca2*	NM_026003.2	18.02
69	*Anxa1*	NM_010730.2	18.00
70	*Hnrnph1*	NM_021510.2	17.90
71	*Tra2b*	NM_009186.4	17.18
72	*Blnk*	NM_008528.4	17.06
73	*Stra6*	NM_001162475.1	17.02
74	*Fkbp9*	NM_012056.2	17.02
75	*Wbp5*	NM_011712.2	17.02
76	*Ehf*	NM_007914.3	16.92
77	*Ddx3x*	NM_010028.3	16.74
78	*Plat*	NM_008872.2	16.56
79	*Ptp4a1*	NM_011200.2	16.34
80	*Tmem131*	NM_018872.2	16.34
81	*Odf2*	NM_001113213.1	16.09
82	*Slc7a5*	NM_011404.3	16.08
83	*Sc5d*	NM_172769.2	16.01
84	*Dfna5*	NM_018769.3	15.94
85	*Nucks1*	NM_001145804.1	15.77
86	*Pcna*	NM_011045.2	15.75
87	*Uba2*	NM_016682.2	15.69
88	*Rbbp7*	NM_009031.3	15.59
89	*Hspd1*	NM_010477.4	15.50
90	*Sox17*	NM_011441.4	15.43
91	*Cdc6*	NM_011799.2	15.42
92	*Cct7*	NM_007638.4	15.38
93	*2610201A13Rik*	AA222883	15.20
94	*Rab18*	NM_181070.5	15.19
95	*Ctsl*	NM_009984.3	15.14
96	*Tsc22d1*	NM_009366.2	14.89
97	*Rcn2*	NM_011992.2	14.86
98	*Brd1*	NM_001033274.3	14.82
99	*Clcn3*	NM_007711.3	14.70
100	*Ptn*	NM_008973.2	14.62
101	*Cma1*	NM_010780.2	14.60
102	*Rbm14*	NM_019869.2	14.51
103	*Chrnb1*	NM_009601.4	14.35
104	*Rps6ka4*	NM_019924.1	14.31
105	*Rbbp4*	NM_009030.3	14.29
106	*Ptma*	NM_008972.2	14.23
107	*Krt6a*	NM_008476.3	14.10
108	*Tnfrsf11b*	NM_008764.3	14.10
	Spp1	NM_009263.2	4.96
	Mmp7	NM_001177352.1	3.07
	Myc	NM_021330.4	2.65
	Cd44	NM_001039150.1	1.38

NOTE. mRNA preparations from the polyps and normal mucosa in the $Apc^{\Delta 716}$ mice were analyzed by DNA microarrays (Affymetrix). The data are expressed as fold-changes in the polyps of $Apc^{\Delta 716}$ mice compared with normal mucosa of $Apc^{\Delta 716}$ mice. Results show the mean (n = 3).

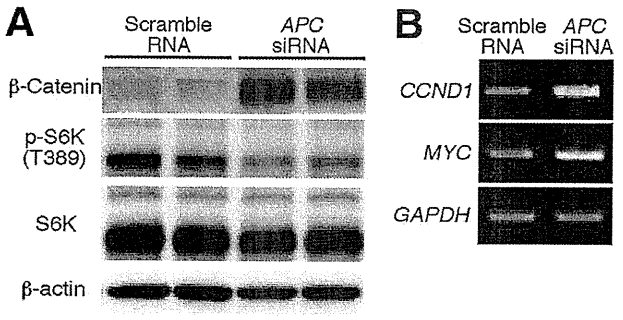

Supplementary Figure 1. mTORC1 signaling was unaffected by Wnt signaling induced by loss of Apc. (*A*) Western blot analysis of p-S6K in RKO colon cancer cells where Wnt signaling was intact and siRNA against *APC* or scramble RNA was treated. (*B*) reverse-transcription polymerase chain reaction (RT-PCR) analysis of Wnt target genes, *CCND1*, and *MYC* in RKO cells treated with siRNA against *APC* or scramble RNA. *Glyceraldehyde-3-phosphate dehydrogenase* is shown as a loading control.

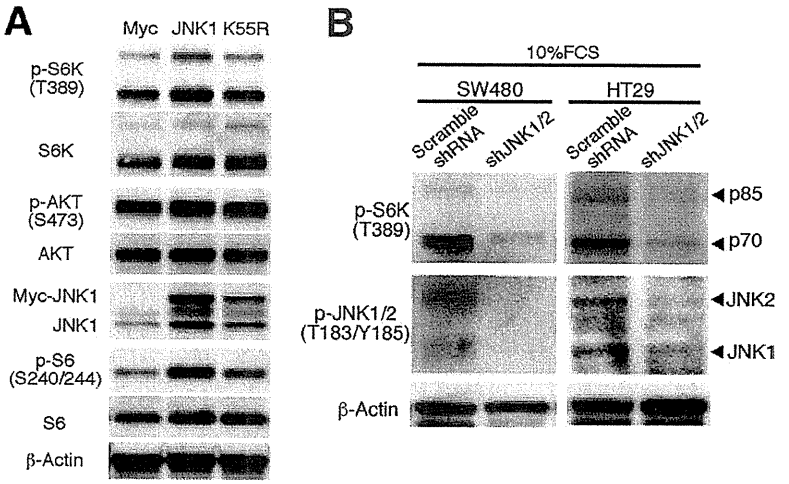

Supplementary Figure 2. JNK activates mTORC1 signaling. (*A*) Western blot analysis of mTORC1 signaling in SW480 cells overexpressing Myc-JNK1 or Myc-K55R. SW480 cells were incubated in a medium containing 10% fetal calf serum (FCS). (*B*) Western blot analysis of p-S6K in SW480 and HT29 cells expressing shRNA against JNK1/2 (sh1) or scramble RNA. Cells were incubated in a medium containing 10% FCS.

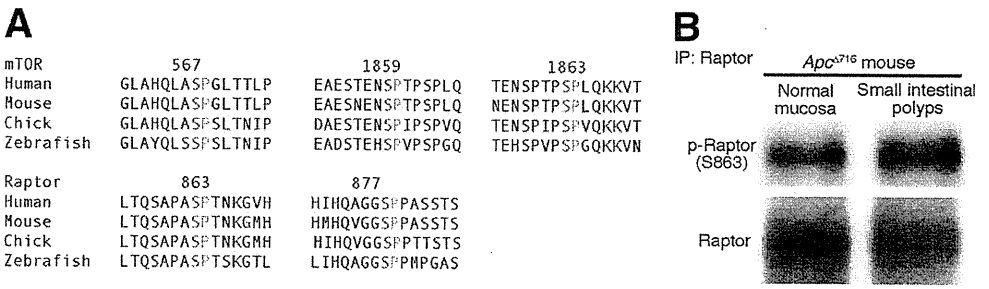

Supplementary Figure 3. JNK phosphorylates mTORC1 component Raptor. (*A*) Amino acid sequence alignments showing conservation of the possible JNK phosphorylation sites, serines, or threonines adjacent to prolines, of mTOR and Raptor orthologs in several species. (*B*) Phosphorylation of Raptor at serine 863 is increased in polyps of $Apc^{\Delta 716}$ mice. The Raptor protein from normal mucosa or polyps in the small intestine of $Apc^{\Delta 716}$ mice was prepared by immunoprecipitation and subjected to Western blot analysis.

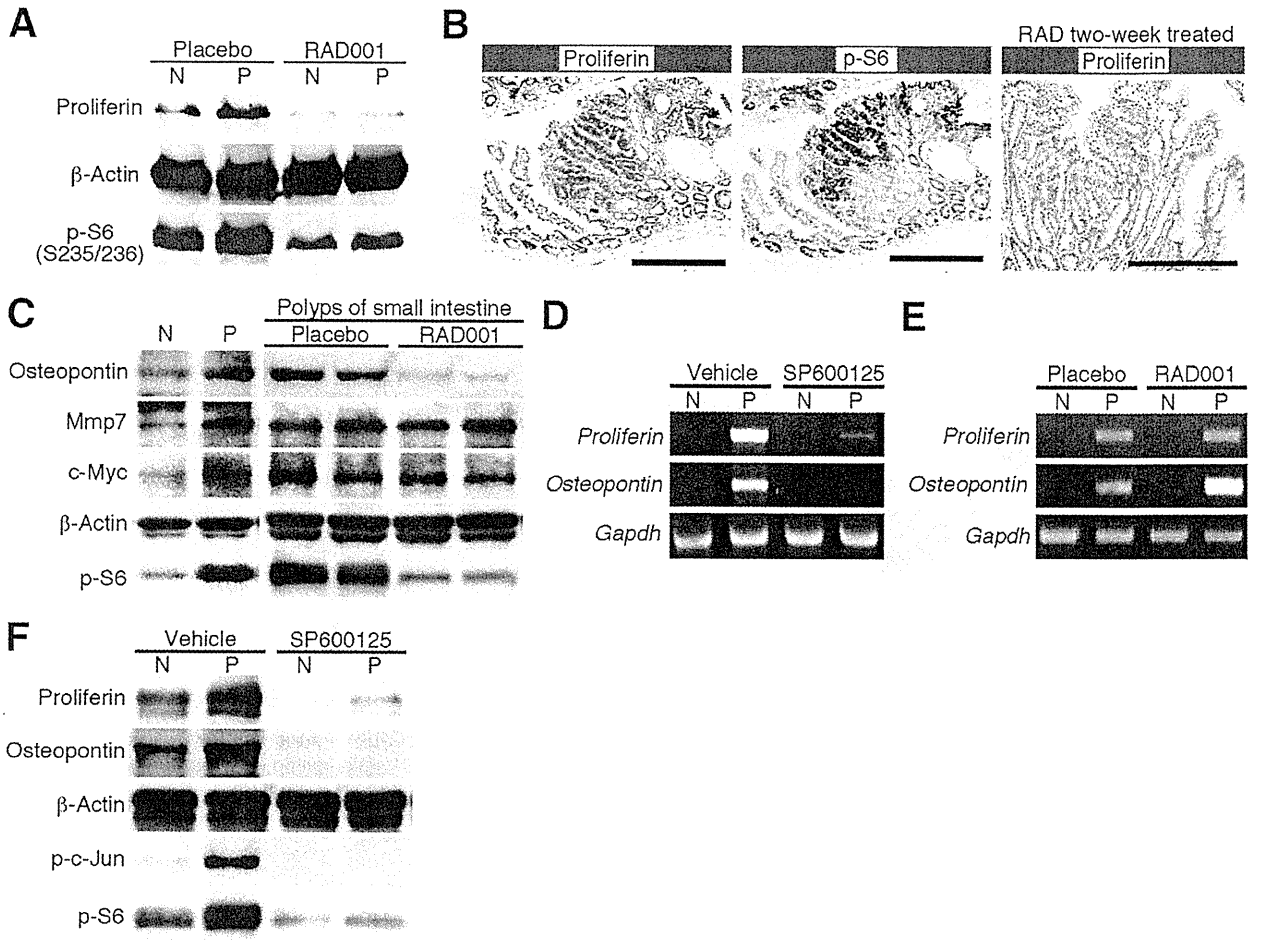

Supplementary Figure 4. JNK/mTOR signaling increased the levels of proliferin and osteopontin in the polyps of $Apc^{\Delta 716}$ mice. (*A*) Western blot analysis of proliferin in normal mucosa or polyps of the small intestine. $Apc^{\Delta 716}$ mice were treated with RAD001 at 10 mg/kg or with placebo for 2 weeks. N, normal mucosa; P, polyps. (*B*) Immunostaining for proliferin (left) and p-S6 (middle) in serial sections of $Apc^{\Delta 716}$ mouse polyp. (Right) Immunostaining for proliferin in a polyp of the $Apc^{\Delta 716}$ mouse treated with RAD001 for 2 weeks. (*C*) Western blot analysis of osteopontin, Mmp7, and c-Myc proteins in normal mucosa or polyps of the small intestine of $Apc^{\Delta 716}$ mice treated with 10 mg/kg RAD001 or with placebo for 2 weeks. N, normal mucosa; P, polyps. (*D*) Reverse-transcription polymerase chain reaction (RT-PCR) analysis of *proliferin* and *osteopontin* mRNAs in normal mucosa or polyps of the small intestine of $Apc^{\Delta 716}$ mice treated with the vehicle or with SP600125 at 50 mg/kg for 2 weeks. N, normal mucosa; P, polyps. (*E*) RT-PCR analysis showing that *proliferin* and *osteopontin* mRNAs in normal mucosa or polyps of the small intestine of $Apc^{\Delta 716}$ mice treated with the placebo or with RAD001 at 10 mg/kg for 2 weeks. N, normal mucosa; P, polyps. (*F*) Western blot analysis of proliferin and osteopontin in normal mucosa or polyps of the small intestine. $Apc^{\Delta 716}$ mice were treated with SP600125 at 50 mg/kg or with placebo for 2 weeks. N, normal mucosa; P, polyps.

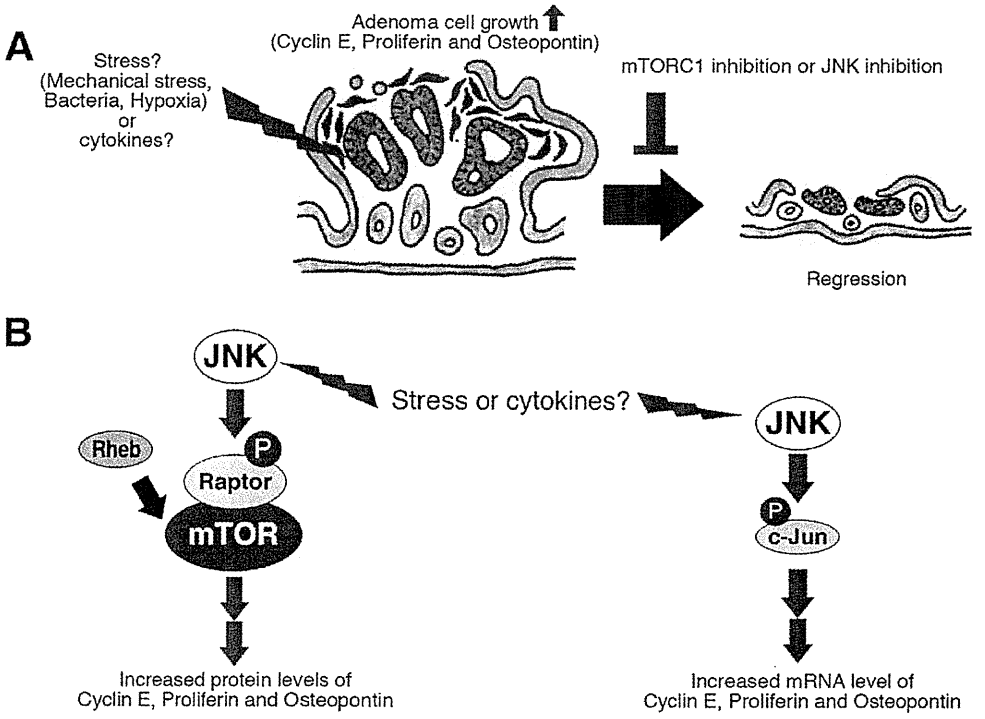

Supplementary Figure 5. JNK activation stimulates mTOR signaling in the intestinal polyps of *Apc*$^{\Delta 716}$ mice. (*A*) JNK activation stimulates mTORC1 signaling, which contributes to the growth of adenoma cells. (*B*) JNK can activate mTORC1 signaling through phosphorylation of Raptor. Activation of JNK helps increase the levels of both mRNA and protein associated with the tumor growth (eg, cyclin E), through stimulation of c-Jun and mTORC1 signaling, respectively.

Exp. Anim. 60(1), 57–63, 2011

—Original—

Kyoto Rhino Rats Derived by ENU Mutagenesis Undergo Congenital Hair Loss and Exhibit Focal Glomerulosclerosis

Takashi KURAMOTO[1)], Mitsuru KUWAMURA[2)], Fumi TAGAMI[1)], Tomoji MASHIMO[1)], Masato NOSE[3)], and Tadao SERIKAWA[1)]

[1)]Institute of Laboratory Animals, Graduate School of Medicine, Kyoto University, Sakyo-ku, Kyoto 606-8501, [2)]Laboratory of Veterinary Pathology, Osaka Prefecture University, Izumisano, Osaka 598-8531, and [3)]Department of Pathogenomics, Graduate School of Medicine, Ehime University, Toon, Ehime 791-0295, Japan

Abstract: *N*-ethyl-*N*-nitrosourea (ENU) mutagenesis is an important tool for studying gene function and establishing human disease models. Here, we report the characterization of a novel hairless mutant rat strain that carries a recessive mutation called Kyoto rhino (*krh*), which was created by ENU-mutagenesis. We produced a F344-*krh* strain through inbreeding without backcrossing to F344 rats. The *krh/krh* rats lost their coat hair by eight weeks of age. They also developed wrinkled skin, cystic hair canals and long curved nails by four months of age. Markedly dilated hair follicles that contained keratin debris were observed during histological analysis of the skin. The *krh* locus was mapped near the hairless (*Hr*) gene on chromosome 15. Sequence analysis revealed a nonsense mutation (c. 1238 C>A, p. S413X) in the *Hr* gene. The truncated HR protein was deduced to lack a zinc-finger domain and repression domains. In aged Hr^{krh}/Hr^{krh} rats, focal glomerulosclerosis (FGS) was observed in which collapsed glomeruli contained protein exudates in Bowman's capsule. Mesangial matrices that had proliferated in segments and foot processes that were fused in podocytes were also observed. The Hr^{krh}/Hr^{krh} rats also suffered from significant proteinuria. Given its breeding history, the F344-Hr^{krh} strain may harbor ENU-induced mutation(s) that underlie FGS in addition to having the Hr^{krh} mutation. The F344-Hr^{krh} rat is a useful model of skin disease and may provide a new model system for the examination of the pathogenesis of FGS.

Key words: disease model, hairless, mutation, nephrosis

Introduction

Hairless mutant rodents are valuable models for studying molecular mechanisms that underlie hair growth control. They are particularly valuable when searching for the genetic basis of hereditary human hair disorders.

In mice, 43 mutations are responsible for primary genetic hairlessness [7]. Among them, the most important are allelic mutations of the hairless (*Hr*) gene. The best characterized allele is the hairless (*hr*). Hr^{hr}/Hr^{hr} mice have a striking total alopecia phenotype which appears between three and four weeks of age. The pheno-

(Received 17 August 2010 / Accepted 16 September 2010)

Address corresponding: T. Kuramoto, Institute of Laboratory Animals, Graduate School of Medicine, Kyoto University, Yoshidakonoe-cho, Sakyo-ku, Kyoto 606-8501, Japan

type originates in the periorbital region and propagates in a wave-like fashion in the rostral-to-caudal direction [20]. It has been determined, through comparative studies of several distinct mouse *Hr* mutations, that the *Hr* gene product plays a key role in controlling hair follicle transformation during the catagen phase [20]. The hairless phenotype of *Hr*-mutant mice (Hr^{hr}/Hr^{hr}) is similar to that of the human disease atrichia. The disease phenotype comprises papular lesions (APL) and alopecia universalis congenital (ALUNC), complete hair loss after birth. It is a result of human *HR* mutation [2, 4, 9].

Another important mutant *Hr* of the mouse is the rhino (*rh*) mouse. Hr^{rh}/Hr^{rh} mice lose all of their hair by seven weeks of age, possess wrinkled skin and their nails overgrow. Additionally, they develop an autoimmune disease characterized by hypergammaglobulinemia, immunoglobulin deposits in the basement membrane of skin, spleen, liver, and kidney, and the presence of antinuclear antibodies which appear in young mice and increase with age [14].

Several rat hair loss mutations have been described. They are for the Charles River hairless rat [1], the Iffa Credo (IC) rat [6], the Hairless Wistar Yagi rat also known as the HWY/Slc rat [13], the Dundee experimental bald rat also known as the DEBR rat [22], the Bald rat [12], and the Hirosaki hairless rat (HHR) [17]. An intragenic deletion in the desmoglein 4 gene underlies the IC rat skin phenotype [6]. The absence of 80-kb of genomic DNA that contains five basic keratin genes is the cause of the HHR rat hairless phenotype [17].

Rat hair follicles are larger than those of mice. Therefore hairless mutant rats are attractive models for studying hair follicle development, differentiation, and cycling. Rat mutants are also good models for evaluating the effects of new drugs for treating human skin diseases. Therefore, it would be beneficial to establish new hairless rat models for these purposes.

We recently treated rats with *N*-ethyl-*N*-nitrosourea (ENU) to obtain different mutants [16]. Several hair loss phenotypes were identified by employing phenotype-driven screening. A hair loss mutant line was established by crossing mutant-type males with wild-type female littermates. Our analysis of the breeding record of this line can be used to prove that the hair loss phenotype is autosomal recessive. Thus, the mutation was named Kyoto rhino (*krh*).

In this study, we identified the *krh* mutation using a positional candidate approach and characterized the *krh/krh* rats. *krh* is a nonsense mutation of the rat *Hr* gene. *krh/krh* rats develop renal failure with massive proteinuria and focal glomerulosclerosis (FGS).

Materials and Methods

Animals

ENU-treated F344/NSlc male rats were mated with F344/NSlc female rats to generate G_1 offspring [16]. The ENU-mutagenized G_1 rats (n=42) were used as founders for the phenotype-driven screening of recessive mutations. Briefly, the G_1 rats were crossed with two F344 rats to generate G_2 offspring. The female G_2 offspring were then backcrossed with their parental G_1 rats to generate G_3 offspring. The recessive mutations induced by ENU in the G_1 rats become homozygous in the G_3 rats. Among the G_3 offspring (n=11) from a G_1 male (#E2307), three rats showed a hair loss phenotype; these rats were probands (P generation). We mated the affected rats with the normal littermates to fix the hair loss phenotype. The phenotype was fixed at the F_2 generation and the mutation was called *krh*. A mutant line was established by employing brother-sister mating (homozygous male × heterozygous female). The generation of inbreeding had reached F_6 at the end of August, 2010. The animal care and experimental procedures that were used were approved by the Animal Research Committee, Kyoto University and were carried out according to the Regulation on Animal Experimentation at Kyoto University.

Genetic mapping

Twenty N_2 rats were produced from a (BN/SsNSlc × F344-*krh/krh*)F_1 × F344-*krh/krh* backcross. The genotypes for the *krh* locus were identified on the basis of coat phenotype at four to five weeks of age. Genomic DNA was prepared from tail biopsies using an automatic DNA purification system (PI-200, Kurabo, Japan) and genotypes for *D15Rat10*, *D15Rat13*, and *D15Rat85* were determined. Linkage relationship was evaluated using the chi-square test of the Excel statistical package.

Confidence intervals ($P<0.05$) were calculated according to the method of a previous report [11].

RT-PCR and direct sequencing

Total RNA was isolated from the skin of five-week-old animals using ISOGEN (NIPPON GENE, Tokyo, Japan). RT-PCR and direct sequencing of the PCR product was carried out as described previously [15]. Rat *Hr* cDNA was amplified using the following eight primer sets: rHr-01&02 CACCTGTGGAAGGCTGCT and ACAGGGTCACTCTTGGGATG; rHr-03&04 AGGGACTACGCTGGAAGGAA and CCCAAACGTTACCGAGAGTG; rHr-05&06 GCAGGCAGCAGAATCTTTG and TCCTGTGGATGTCTCTGGTG; rHr-07&08 ACTCAAGAGGGCAGGCAGT and GGTGTTGAAGAGTCCGTGGT; rHr-09&10 CTTCCATCAACAAGGGCCTA and CTGGGCTCTCTGTGGAGTCT; rHr-11&12 GGTCAGCAGAAGGAACCAAC and TTCCAGAATGCTGTGCTGTC; rHr-13&14 GACTTAGCCTGTGGGGAATG and CTCCAAGGTTCCTGCTCCAG; rHr-15&16 GTCTCCAGGTAGCCAGACCA and GTTCCCTGCTTGTACCCAAA. The PCR products overlapped each other and spanned the entire 3,624 bp *Hr* coding sequence (CDS).

Morphological analysis

Dorsal and ventral skin samples were collected from *krh/krh* and *krh/+* littermates at two, nine and seventeen weeks of age. Mouse anti-cytokeratin (AE1/AE3, Dako Japan, Tokyo, Japan) was used for immunohistochemical analysis of the skin samples. Bound antibody was detected using horseradish peroxidase conjugated anti-mouse antibody (Histofine Simplestain MAX-PO; Nichirei, Tokyo, Japan) and 3,3'-diaminobenzidine as a chromogen (Vector Laboratories, Burlingame, CA, USA). To detect lipids, frozen sections were made from specimens that had been fixed with formalin and they were stained with Oil red O.

Organ samples of the heart, lungs, liver, pancreas, kidneys, spleen, lymph nodes, salivary glands, lacrimal glands, thyroid gland, adrenal glands, small and large intestines, and knee and foot joints, were collected from three *krh/krh* rats and three F344 rats at 40 weeks of age. They were fixed using 10% neutral buffered formalin, embedded in paraffin, cut at 4 μm in thickness, and then stained with hematoxylin and eosin (HE). To study glomerular lesions, periodic acid-Schiff (PAS) or periodic acid-methenamine-silver (PAM) staining was employed. For immunofluorescence studies, kidney samples were frozen in 22-oxacalcitriol compound (Miles Inc., Elkhart, IN, USA).

Electron microscopy

Perfusion fixation through the left ventricle was conducted with 4% paraformaldehyde in 0.1 M phosphate buffer (PB). Kidneys that had been excised were stored in 2% paraformaldehyde and 2.5% glutaraldehyde in 0.1 M PB. They were fixed with 2% osmic acid for 2 h and embedded in epoxy resin. Ultra-thin sections were double-stained with uranyl acetate and lead citrate and examined using a Hitachi H-7500 electron microscope (Hitachi, Tokyo, Japan).

Urine protein measurement

To collect urine, six male *krh/krh* rats and six F344/NSlc (+/+) rats, 40 weeks of age, were caged individually in metabolic chambers after they had been orally loaded with physiological saline at 2.5 ml/100 g body weight. Six-hour urine samples were collected and their volumes, and protein concentrations were determined. Statistical differences were determined using the Mann-Whitney U test.

Results

krh/krh rat hair loss phenotype and skin morphology

For the *krh/krh* rats, hair loss first occurred around the nose around 2 weeks after birth and extended gradually from the anterior to the posterior of the body (Fig. 1A and 1B). At around four months of age they had wrinkled skin, cystic hair canals and long curved nails.

Through histopathological analysis, markedly dilated hair follicles were observed. These cystic follicles contained a lot of keratin debris (Fig. 1C), and they stained positive for cytokeratin (Fig. 1D). The cysts were lined by a thin layer of squamous epithelium and an easily identifiable granular cell layer. The sebaceous glands that surrounded the dilated cysts were hyperplastic. Staining with Oil red O revealed that a large amount of lipids was present in the lumen of each cyst and on the

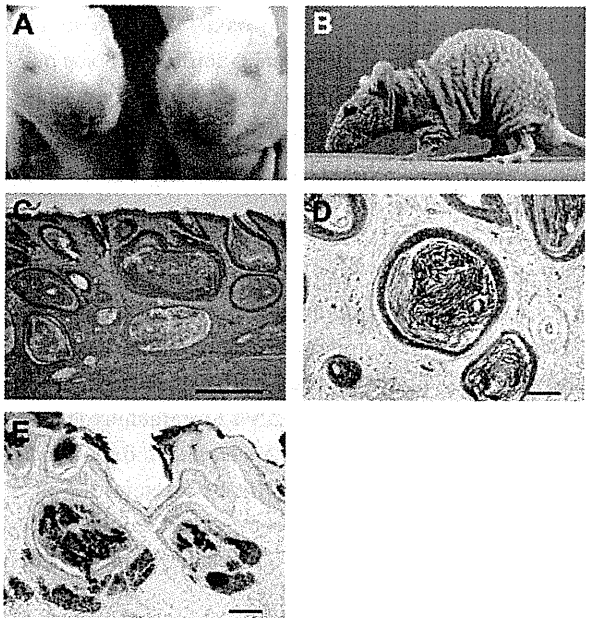

Fig. 1. Phenotypic and morphological characteristics of the Kyoto rhino rat. A: Right; a 2-week-old *krh/krh* rat with characteristic hair loss on the snout. Left; a littermate *krh/+* rat. B: Rhinocerotic appearance of a 10-week-old *krh/krh* rat. C: Histopathology of 9-week-old *krh/krh* rat skin. HE staining. Bar=500 μm. D: IHC of keratin of a 9-week-old *krh/krh* rat. Bar=100 μm. E: Oil Red O staining of a 17-week-old *krh/krh* rat. Bar=100 μm.

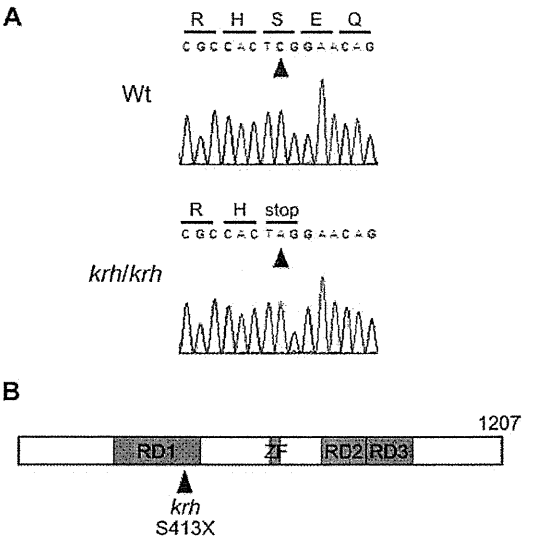

Fig. 2. Identification of the *krh* mutation. A: Results of direct sequencing of *Hr* cDNA of wild-type and *krh/krh* rats. The C-to-A nonsense mutation at position 1,238 is indicated by red arrowheads. The substitution produces a stop codon at amino acid residue 413 of protein HR. B: Schematic of the conserved domains in rat protein HR. RD1, RD2, and RD3 are used to denote the repression domains and ZF is used to denote the zinc-finger domain. The mutation site Ser413Ter is noted with a red arrowhead.

surface of the epidermis (Fig. 1E). These findings are indicators that the *krh/krh* skin and hair phenotypes are similar to those of *rh* at the *Hr* locus of the laboratory mouse [7].

krh is an Hr nonsense mutation

Hr on Chr 15 was believed to be the best candidate for *krh* and therefore the genotype of the backcross progeny was determined using genetic markers for Chr 15. We obtained 12 *krh/krh* and 8 *krh/+* rats from the (BN/SsNSlc × F344-*krh/krh*)F_1 × F344-*krh/krh* backcross. A significant linkage relationship was observed between *krh* and *D15Rat10* (42.7 Mb) with no recombination (χ^2=21.6, P<0.01), which is indicative that *krh* is located <13.9 cM away from *D15Rat10* with 95% probability [11]. *krh* was expected to span from 28.8 Mb to 56.6 Mb of Chr 15, within which the *Hr* locus (50.9 Mb) was mapped (RGSC v3.4).

Sequencing analyses of *Hr* cDNA obtained from *krh/krh* skin samples revealed that adenine (A) had been substituted for cytosine (C) at nucleotide position 1,238 from the start of the CDS (c. 1,238 C>A). This substitution resulted in a stop codon at amino acid 413 of the HR protein (p. Ser413Ter) (Fig. 2A). The truncated HR protein lacked a zinc-finger domain, a part of repression domain (RD) 1, and all of RD2 and RD3 (Fig. 2B). We characterized *krh* as an *Hr* nonsense mutation and called it Hr^{krh}.

Focal glomerulosclerosis and proteinuria in the aged Hr^{krh}/Hr^{krh} rat

Histopathological examinations of organs that were taken from Hr^{krh}/Hr^{krh} rats at 40 weeks of age were performed. No lesions that are associated with autoimmune diseases were observed, however, prominent glomerular lesions were noted in the kidneys of the Hr^{krh}/Hr^{krh} rats. These lesions were focal lesions that had collapsed glomeruli and protein exudates in Bowman capsule and the renal tubules (Fig. 3A and 3C), and segmental prolifera-

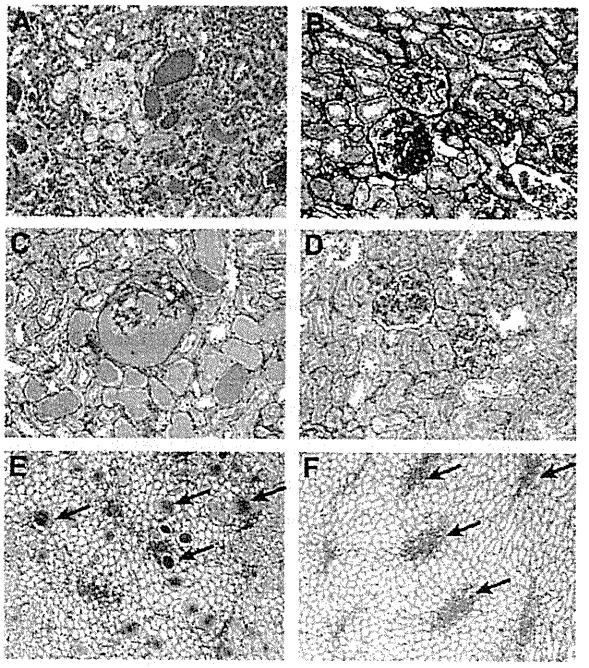

Fig. 3. Focal glomerular sclerotic lesions in 40-week-old Hr^{krh}/Hr^{krh} rat. Note that a collapsed glomerulus with protein exudates in Bowman's capsule and protein casts in renal tubules (A, C), and segmental proliferation of mesangial matrices (B, D) were seen. In the renal medulla, protein casts were notable in the collecting tubules (E) (arrows), but those in a wild-type F344 rat (+/+) were limited only to Henle's loop (F) (arrows). A: HE; B: PAM; C–F: PAS staining.

tion of the mesangial matrices (Fig. 3B and 3D). There was no inflammatory cell infiltration into the glomeruli and interstitium. In the renal medulla, protein casts were notably present in the collecting tubules (Fig. 3E). For the wild-type rats, protein casts were only observed in Henle's loop, possibly due to the effects of aging (Fig. 3F). These findings are indicators that the lesions that were observed in the F344-Hr^{krh}/Hr^{krh} rat were caused by focal glomerulosclerosis (FGS). Moreover, Hr^{krh}/Hr^{krh} rats at 40 weeks of age had proteinuria. The Hr^{krh} homozygous rats had significantly higher urine protein concentrations than age-matched wild-type rats: 152 ± 80.3 vs. 51.0 ± 38.5 mg/dl, (average ± SD), $P<0.02$ (Fig. 4).

From the electron microscopic observations, the segmental glomerular sclerotic lesions were characterized as having proliferating mesangial matrices (Fig. 5A). The proliferation was associated with the dendritic pro-

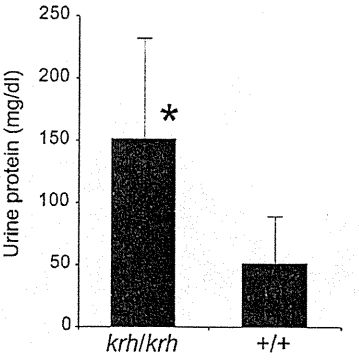

Fig. 4. Urine protein concentrations of Hr^{krh}/Hr^{krh} rats and wild-type F344 (+/+) rats. The Hr^{krh} homozygous rats had significantly higher urine protein concentrations than age-matched wild-type rats. Bars indicate standard deviation. *: $P<0.02$.

cesses of mesangial cells and on rare occasions with dense deposits in the mesangial regions. Foot process fusion was often observed in these glomeruli (Fig. 5B).

Discussion

The *krh* mutation was identified as an *Hr* nonsense mutation and therefore called Hr^{krh}. Protein HR is a nuclear receptor co-repressor for multiple nuclear receptors, such as the thyroid hormone receptor and the vitamin D receptor [23]. In the hair follicle (HF), the absence of functioning HR proteins results in the synthesis of premature and dysregulated catagen. This results in the destruction of the normal HF architecture and abrogates the HF's ability to cycle [20]. The Hr^{krh}/Hr^{krh} rat has cystic hair follicles and suffers from a premature hair cycle (Fig. 1). The truncated HR protein that is encoded by the Hr^{krh} nonsense mutation is caused by a lack of functional domains which play important roles in regulating target genes [23]. Additionally, the mutation may cause nonsense mediated mRNA decay. Therefore, it is likely that Hr^{krh} may be a loss-of-function mutation. In humans, *HR* mutations are associated with congenital alopecia, such as ALUNC and APL [2, 4, 9]. Because rats are suitably sized for handling and manipulating [5, 21], the Hr^{krh}/Hr^{krh} rat may be a useful animal model for developing therapies for these human diseases.

The aged Hr^{krh} homozygous rat has FGS which is as-

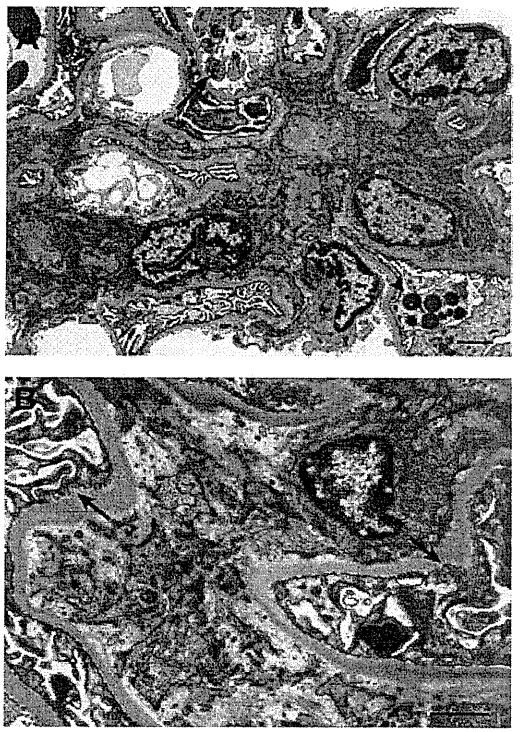

Fig. 5. Fine structures of glomerular lesions in the Hr^{krh}/Hr^{krh} rat. A: Proliferative lesions of mesangial matrices associated with significant dendritic projections from mesangial cells. Platelet aggregation was observed in a capillary loop (arrow). Intracellular hyaline droplets were significant in a podocyte (arrowhead). B: Foot process fusion (arrows) and a proliferative lesion of mesangial matrices that was not associated with dense deposits in mesangial regions and the glomerular basement membrane. Bar: 2 μm.

sociated with severe proteinuria. FGS is a descriptor for a pathological finding in the kidneys. When a nephritic range of proteinuria is observed, patients are diagnosed as having focal segmental glomerulosclerosis (FSGS). FSGS is classified by morphological variants including collapsed glomeruli, cellular proliferation, tip lesions, and diffuse mesangial proliferation [10]. The lesions that were observed in the F344-Hr^{krh} rat are characteristic of collapsed glomeruli associated with protein exudates in Bowman's capsule and may involve a collapsed variant of FSGS. Thus, the F344-Hr^{krh} rat may have potential as a model of nephritic FSGS.

FGS has not been reported for the APL or ALUNC family, and *Hr*-mutant mice, [2, 3, 7]. It is believed that FGS has a heterogeneous etiology and that it may manifest through multiple genetic factors [10]. The F344-Hr^{krh} rats were derived by employing ENU mutagenesis. The founder animals (G_1 generation) were expected to carry no more than four ENU-induced mutations in their CDS, if the CDS occupies 1% of the genome [16]. The F344-Hr^{krh} rats were mated by inbreeding without backcrossing to F344 rats to eliminate ENU-induced mutations other than the Hr^{krh} mutation. Thus, it is likely that the F344-Hr^{krh} rat may harbor mutation(s) that may play a role in the pathogenesis of FGS. FGS in Hr^{krh}/Hr^{krh} rats might be caused by unidentified mutation(s) that were induced by ENU or the combined effects of such mutation(s) with the Hr^{krh} mutation.

The Hr^{rh}/Hr^{rh} mouse has the nonsense mutation (R597X) [8] and develops hypergammaglobulinemia. The excess immunoglobulins that are produced due to this disease are deposited in the basement membranes of the skin, spleen, liver, and kidney, and antinuclear antibodies are produced. These symptoms appear in young mice and increase in severity with age [14]. Although the F344-Hr^{krh}/Hr^{krh} rat has a nonsense mutation (S413X), the mutation is not associated with an autoimmune disease or IgM, IgG, and C3 deposition in the kidneys (data not shown). Generally, pathological phenotypes that are associated with this disease are often influenced by a predisposed genetic background [18, 19]. Therefore, genes that are predisposed to causing autoimmune diseases in *rh/rh* mice may be absent in F344-Hr^{krh} rats. By replacing the genetic background of F344-Hr^{krh} with those of other rat strains, we might find autoimmune disease in Hr^{krh}/Hr^{krh} rats.

In summary, a novel rat mutant strain, F344-Hr^{krh}, was established that carries an *Hr* nonsense mutation (S413X). In addition to the hair loss phenotype, Hr^{krh} homozygous rats suffer from proteinuria and FGS. Therefore, F344-Hr^{krh} may have potential as a model of skin disease as well as nephritic FSGS.

Acknowledgments

This work was supported in part by Grants-in-aid for Scientific Research from the Japan Society for the Promotion of Science (21300153 to TK) and a Grant-in-aid for Cancer Research from the Ministry of Health, Labour